

AD-A140 849

**SHEAR WAVE GENERATION
OF NEAR SURFACE SPALL**

Eric Rinehart

March 1984

Final Report

Approved for public release; distribution unlimited.

20000803062

AIR FORCE WEAPONS LABORATORY
Air Force Systems Command
Kirtland Air Force Base, NM 87117

Reproduced From
Best Available Copy

84 05 07 152

DTIC FILE COPY



This final report was prepared by the Air Force Weapons Laboratory, Kirtland Air Force Base, New Mexico, under Job Order ILIR8308. Dr Eric J. Rinehart (NTED) was the Laboratory Project Officer-in-Charge.

When Government drawings, specifications, or other data are used for any purpose other than in connection with a definitely Government-related procurement, the United States Government incurs no responsibility or any obligation whatsoever. The fact that the Government may have formulated or in any way supplied the said drawings, specifications, or other data, is not to be regarded by implication, or otherwise in any manner construed, as licensing the holder, or any other person or corporation; or as conveying any rights or permission to manufacture, use, or sell any patented invention that may in any way be related thereto.

This report has been authored by employees of the United States Government. Accordingly, the United States Government retains a nonexclusive, royalty-free license to publish or reproduce the material contained herein, or allow others to do so, for the United States Government purposes.

This report has been reviewed by the Public Affairs Office and is releasable to the National Technical Information Service (NTIS). At NTIS, it will be available to the general public, including foreign nations.

If your address has changed, if you wish to be removed from our mailing list, or if your organization no longer employs the addressee, please notify AFWL/NTED, Kirtland AFB, NM 87117 to help us maintain a current mailing list.

This report has been reviewed and is approved for publication.

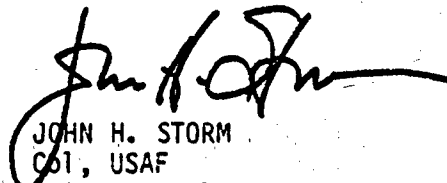


ERIC J. RINEHART
Project Officer

FOR THE COMMANDER



T. D. MCCARSON
Lt Col, USAF
Chief, Technology Branch



JOHN H. STORM
Col, USAF
Chief, Civil Engineering Research Div

DO NOT RETURN COPIES OF THIS REPORT UNLESS CONTRACTUAL OBLIGATIONS OR NOTICE ON A SPECIFIC DOCUMENT REQUIRES THAT IT BE RETURNED.

UNCLASSIFIED

SECURITY CLASSIFICATION OF THIS PAGE

REPORT DOCUMENTATION PAGE			
1a. REPORT SECURITY CLASSIFICATION Unclassified		1b. RESTRICTIVE MARKINGS	
2a. SECURITY CLASSIFICATION AUTHORITY		3. DISTRIBUTION/AVAILABILITY OF REPORT Approved for public release; distribution unlimited.	
2b. DECLASSIFICATION/DOWNGRADING SCHEDULE		5. MONITORING ORGANIZATION REPORT NUMBER(S)	
4. PERFORMING ORGANIZATION REPORT NUMBER(S) AFWL-TR-83-108		7a. NAME OF MONITORING ORGANIZATION	
6a. NAME OF PERFORMING ORGANIZATION Air Force Weapons Laboratory	6b. OFFICE SYMBOL (If applicable) (NTED)	7b. ADDRESS (City, State and ZIP Code)	
6c. ADDRESS (City, State and ZIP Code) Kirtland AFB NM 87117		3. PROCUREMENT INSTRUMENT IDENTIFICATION NUMBER	
8a. NAME OF FUNDING SPONSORING ORGANIZATION	8b. OFFICE SYMBOL (If applicable)	9. SOURCE OF FUNDING NOS.	
8c. ADDRESS (City, State and ZIP Code)		PROGRAM ELEMENT NO. 61101F	PROJECT NO. ILIR
		TASK NO. 83	WORK UNIT NO. 02
11. TITLE (Include Security Classification) SHEAR WAVE GENERATION OF NEAR SURFACE SPALL (U)			
12. PERSONAL AUTHOR(S) Rinehart, Eric			
13a. TYPE OF REPORT Final Report	13b. TIME COVERED FROM Oct 82 to Oct 83	14. DATE OF REPORT (Yr, Mo, Day) 1984, March	15. PAGE COUNT 43
16. SUPPLEMENTARY NOTATION			
17. COSATI CODES		18. SUBJECT TERMS (Continue on reverse if necessary and identify by block number)	
FIELD 20	GROUP 11	Spall	
		Material Properties	
20	14	HEST relief waves	
19. ABSTRACT (Continue on reverse if necessary and identify by block number) Very near field data have been obtained from several in situ, dynamic material properties tests. The explosive driver of the tests was either a rectangular or circular explosive array placed on the surface and covered with an earthen berm. The tests were fired over several different types of alluvium. Following the initial compression and partial rebound, acceleration wave forms show -1 g dwells followed by an impulsive rejoin. This has been identified as spall. The spall appears to be caused by shear waves initiating from the finite edges of the explosive source. The shear waves tend to force the material, both under and beyond the explosive array, upward until the soil fails and falls with a -1 g acceleration. The alluvium beneath the charge remains in compressive strain throughout the entire spall signature. Calculations have verified this mechanism. The planar explosive array may be thought of as an approximation to a surface point source. This would suggest that shear waves are a viable mechanism for spall observed near surface burst experiments.			
20. DISTRIBUTION/AVAILABILITY OF ABSTRACT UNCLASSIFIED/UNLIMITED <input type="checkbox"/> SAME AS RPT. <input type="checkbox"/> OTIC USERS <input checked="" type="checkbox"/>		21. ABSTRACT SECURITY CLASSIFICATION Unclassified	
22a. NAME OF RESPONSIBLE INDIVIDUAL Dr Eric Rinehart		22b. TELEPHONE NUMBER (Include Area Code) (505) 844-0861	22c. OFFICE SYMBOL AFWL/NTED

DD FORM 1473, 83 APR

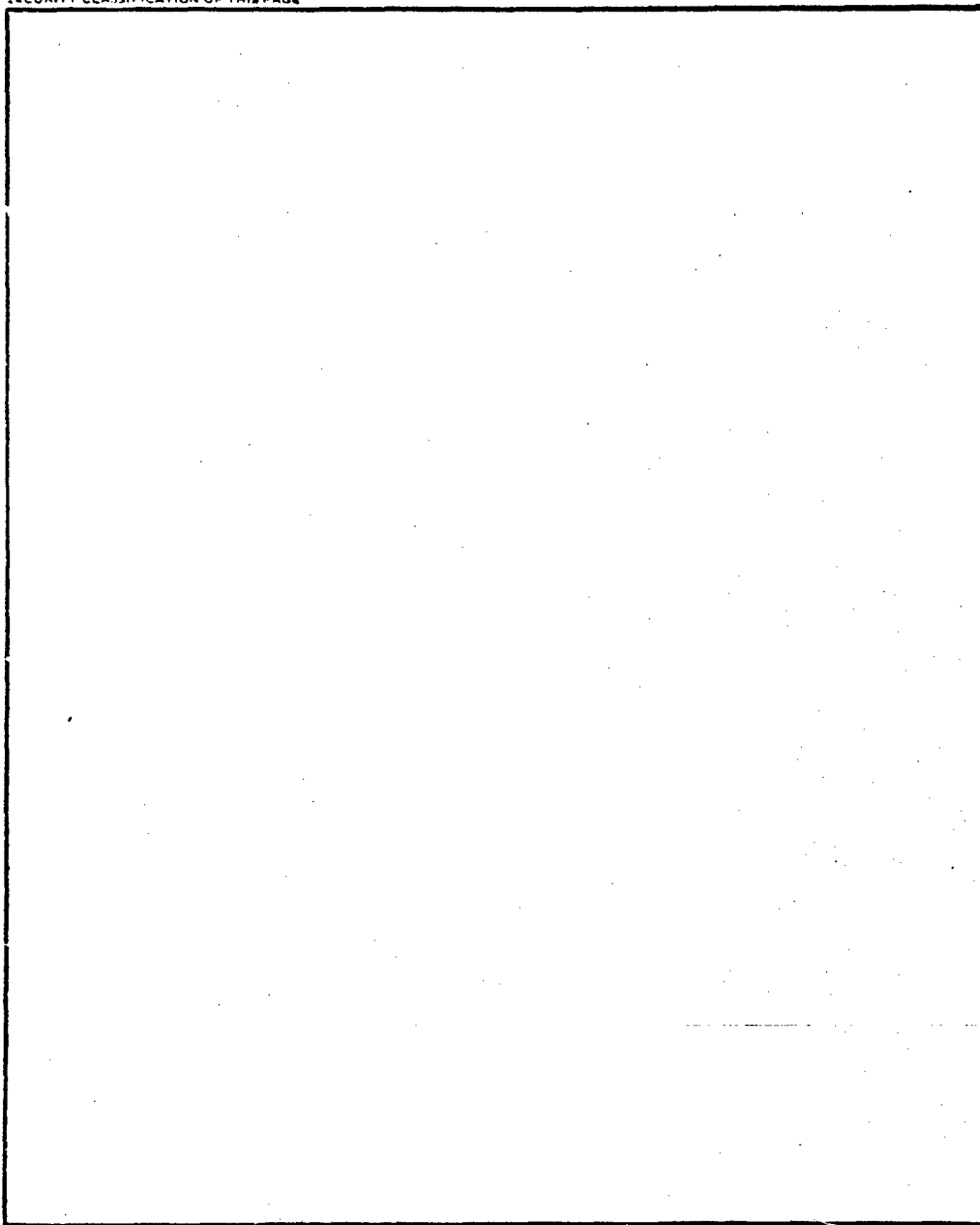
EDITION OF 1 JAN 73 IS OBSOLETE.

UNCLASSIFIED

SECURITY CLASSIFICATION OF THIS PAGE

UNCLASSIFIED

SECURITY CLASSIFICATION OF THIS PAGE



UNCLASSIFIED

SECURITY CLASSIFICATION OF THIS PAGE

CONTENTS

<u>Section</u>	<u>Page</u>
I INTRODUCTION	1
II SPALL MECHANISM	3
III DATA ANALYSIS	6
IV CALCULATIONS	11
V DISCUSSION AND CONCLUSION	15
REFERENCES	36



Accession for	
NTIS GRA&I	<input checked="" type="checkbox"/>
DTIC TAB	<input type="checkbox"/>
Unannounced	<input type="checkbox"/>
Justification	
By	
Distribution/	
Availability Codes	
Dist	Avail and/or
A1	Special

I. INTRODUCTION

For the past several years, planar explosive charge arrays have been detonated on the earth's surface for the purpose of subjecting a test-bed to compressional stress while retaining uniaxial strain. These High Explosive Simulation Technique (HEST) tests are useful in providing dynamic in situ compressional data for determining uniaxial strain versus stress equations of state for various earth materials. (Bratton and Higgins, 1979 (Ref. 1): Swartz, et al, 1981 (Ref. 2) and Jackson and Zelasko, 1982 (Ref. 3)). In addition, planar explosive arrays also have been used to approximate the overhead airblast impulses produced from surface point charges. The limited practical size of a HEST test-bed (Fig. 1) causes nonuniaxial strain effects to be generated by the finite test-bed edges. Generally, the test-bed edges cause volumetric stress release waves (named P release waves) and rotational or deviatoric stress waves (S release waves) inside the test-bed (Rinehart and Lucey, 1981 (Ref. 4)). The two release waves assist in releasing the uniaxial soil stress to a natural state of lithostatic stress. Beyond the edge of the HEST boundary, the first recorded motion is compressional in nature and is followed by the deviatoric or shear wave.

Previous interest has generally been focused on the short duration (tens of millisecond) initial compressional cycle of uniaxial strain beneath the HEST. Attempts have been made in understanding the edge release effects in order that the arrival time of perturbations from uniaxial strain could be estimated. The HEST would then be sized to guarantee uniaxial flow for specified periods of time within the test-bed. As late time data became available, it became evident that in dry alluvium the release waves produced stresses and strains on the same order as the initial compressional phase. To completely understand cause and effects of soils and structures in the test-bed, an understanding of the release waves was necessary. Of particular interest in this study are the late time effects of the release waves both beneath the HEST and beyond its finite boundaries. Constructive uses of these effects for material modeling have been identified.

Long durations (up to 1 s) of acceleration and velocity time histories from several HESTS fired in dry alluvium (Fig. 2) show the edge release effects. In all cases, the final resulting release signals lead to wave

signatures that contain -1 g dwells and rejoin. The -1 g dwells indicate that the soil is in free flight under tensional failure; the material has spalled from the original surface. Similar waveforms, identified as spall, have been observed in data obtained from surface high explosive bursts (Stump and Reinke, 1983 (Ref. 5); Merkle, 1980 (Ref. 6) and Parret, 1978 (Ref. 7)).

The waveforms include initial compression followed by release of the stress. The data show that stress release caused by the edge of the explosive cavity is so severe that the soil frequently attains upward velocity. For all records obtained for dry alluvium, the upward velocity leads to material failure and free fall (-1 g in acceleration) ending in rejoin of the material. This spall initiates in such a manner that the classical spall mechanism of compressional wave reflection (Rinehart, 1959 (Ref. 8); Eisler and Chilton, 1964 (Ref. 9); Viecelli, 1973 (Ref. 10)) initiating the spall, is not supported by the observations. Data and calculations suggest that large magnitude shearing actions caused by the HEST edges is the probable cause of the observed spall.

The primary objective of this work is to identify and quantify the mechanism of spall initiation caused shearing motions. The mechanism will be addressed through wave ray tracing techniques and comparison of the data to two dimensional finite difference calculations. In addition, a limited parameter study was done with the finite difference calculations to quantify effects caused by changes in shearing properties. Finally, some thoughts are presented on extending these results to spall phenomena observed on high explosive surface bursts.

II. SPALL MECHANISM

Spall waveforms are a result of tensional failure of in situ material (Rinehart, 1975 (Ref. 11)). Early workers (Rinehart, 1959 (Ref. 8); Eisler and Chilton, 1964 (Ref. 9) and Viecelli, 1973 (Ref. 10)) usually associated the tensional failure with a tensional reflection from a free surface of a compressional wave, although, Chilton, et al (1966) (Ref. 12) and Parret (1978) (Ref. 7) attribute some spall records observed for buried sources in alluvium to excessive compaction of the alluvium itself.

Most early observations of spall were obtained from tests in hard rock, metals, or other materials where tensile failure results in a finite failure surface. The source produces a high amplitude compressive shock wave that travels from the source to a free surface. Upon reflection from the free surface, a tensile wave is superposed onto the compressive wave until the total stress exceeds the tensile limit of the material. The upper spalled layer then goes into free flight (-1 g dwell) and is followed by a sharp rejoin. The wave travel time curves for classical spall show initial compression traveling from the source to the free surface and spall or tensional failure traveling from the free surface to the source. Based upon this physics, Stump and Reinke (1983) (Ref. 5) have proposed criteria upon which spall can be identified.

PRIMARY CRITERIA

- a. Minus 1 g (allowable range -0.5 g to -2.0 g) vertical acceleration dwell. (Assumes accelerometers are calibrated to read zero g in the earth's gravitational field.)
- b. Impulsive material rejoin signals on all components.
- c. No acceleration dwells on horizontal components.

SECONDARY CRITERIA

- a. Dwell times of some duration.
- b. Amplitudes of rejoin.

These criteria were used throughout this work and are adequate for spall identification regardless of the initiation process.

Using the above criteria Stump and Reinke (1983) (Ref. 5) and Parret (1978) (Ref. 7) have identified spall that does not appear, through arrival time considerations, to be a result of the classical phenomenon. The spall signals result from both buried sources and from surface point sources. As a result of the inadequacy of the classical spall mechanism to predict their observations, Stump and Reinke (1983) (Ref. 5) have proposed four additional mechanisms which provide a physically realizable source for the required tensional wave and failure. These include:

1. Rayleigh/shear waves from surface sources--a wave equation effect.
2. Spherical or cylindrical divergence of the wave field--a geometric effect.
3. Granular soil pore-air expansion effect--either a source or material property effect.
4. Material compaction and evacuated cavity--a material property effect.

Details of these mechanisms are found in Stump and Reinke (1983) (Ref. 5) and Parret (1978) (Ref. 7). A comparison of different spall mechanisms is shown in Figure 2. The top waveform clearly shows the features of classical spall. The source is an underground 115 kg sphere of high explosive buried 11.8 m beneath the surface. The record is taken from a station between the source and the surface and shows the arrival of the initial compressional wave forcing the material upward followed by a sharp reversal and -1 g dwell. The reversal indicates the arrival of the reflected tensile wave and material failure. Note the sharp arrivals of both the initial compression and tensile stresses. Also note the rapid reduction of the acceleration to -1 g. The second record in Figure 2 is recorded from a surface bermed 38 kg explosive sphere. The record is taken just beneath the surface at a radial distance of a few meters from the source. Initial motion is upward followed by a series of arrivals that result in a -1 g condition labeled as spall (Stump and Reinke, 1983 (Ref. 5)). The source of the tensional failure is believed by Stump and Reinke (1983) (Ref. 5) to be an arrival of a shear wave. Note the difference

in initiation of the spall phase. The buried charge record has a sharp reversal, while the surface burst has a slower, less distinct beginning of the spall. These two records, while both showing spall, have very different proposed mechanisms. The remaining four records are recorded beneath various planar HEST tests (Table 1). For these records, the initial phase is downward compression followed by stress release and a slow initiation of the spall. The spall portion of the records is quite similar to the PHG-79-6 data, including the slow initiation of the -1 g dwell, rather than the sharp initiation seen in the buried shot shown. (As pointed out by Parret (1978) (Ref. 7) however, nonclassical spall phenomena has been observed for two buried explosions.) The slow initiation of spall, in itself, suggests that a mechanism other than classical spall is working in the HEST test-bed.

For surface point sources, the shear component of the stress tensor is an important source of energy (Aki and Richards, 1980 (Ref. 13)) as compared to a buried source. Stump and Reinke (1983) (Ref. 5) showed that the shear component created by a point surface charge produces substantial tensional stress, which when exceeding any tensile failure limit of the soil would result in free fall. Present HEST data show spall in the subsurface region below the test-bed having similar characteristics to a point surface charge, suggesting a shear mechanism. Spall, as will be seen, is also present outside of the test-bed. Some finite difference calculations also suggest a shear source.

III. DATA ANALYSIS

The data used in this report were obtained from motion measurements from HEST experiments. The explosive array consists of an explosive and bead foam mixture overlaid with a soil berm. Upon detonation, the explosive and foam mix and berm to provide a peak gas pressure, dependent upon the total charge weight, within a cavity contained by the berm on top and soil underneath the cavity. The weight of the berm controls the decay of the peak pressure or pressure impulse. With a foam and explosive mixture, peak obtainable pressures are much less than the peak pressures produced by detonation of the explosives alone. For material properties determination, HESTs generally are circular (DH-1, DISC-1 and DISC-2); although rectangular or square designs have also been used (SIMCAL III and DAT-3) (Table 1). Motions beneath the test-bed are usually measured with high g accelerometer packages having uniaxial, biaxial, or triaxial capabilities. The accelerations are then integrated to give velocities and displacements. In a uniaxial strain environment, motion measurements alone are adequate for complete determination of both motion and stresses. However, for the relatively late times of interest for spall observations the strains are no longer uniaxial. In this case both motions and stresses cannot be uniquely determined from motion gages. For complete determination of the stress field, both normal and shear stress measurements are required. The state of the art does not presently allow these measurements; indeed, normal soil stress measurements are usually suspect in dry alluvial material. As a result, soil stress is not a parameter that can be used quantitatively in this analysis.

For a recording station at Point A (Fig. 1), beneath the explosive cavity, the wave arrivals can be predicted using calculations. The initial motion is vertical, downward uniaxial compression. Directly following the initial compression is the P wave caused by the finite boundary, Point B (Fig. 1), of the HEST. Motion from the P wave is upward and outward within the test-bed. Outside of the test-bed the P wave is compressional in nature. The next arrival is the edge generated shear wave, also imparting an upward motion, and inward particle velocity within the test-bed and down and outward velocities outside of the test-bed. Point A is also affected by the release waves from the boundary on the opposite side of the HEST. For simplicity the opposite

edge release waves are considered to be reflections from the center line of the test-bed. The position of Point A and the various wave speeds determine the relationship between the arrivals of the various release waves. On the center line, both P waves and both S waves arrive simultaneously. In addition to the primary P and S waves, there are P to S conversions that appear as diffracted waves, with emergent arrivals whose arrival times can only be estimated.

Note that beneath the test-bed, all of the release waveforms have motions that imply stress release and upward motion. In other words, under the explosive, velocity reduction and return to the lithostatic stress state is a superposition of the cavity pressure decay plus the reversal due to the finite size of the HEST.

Acceleration waveforms recorded approximately 3 m out from the center line of DH-1 for 4.0 m to 13.0 m depths (Fig. 3) are seen to contain a multitude of arrivals, peaks and troughs. Based on knowledge of the wave speeds (Table 2) and initial motions, an attempt was made to pick out individual arrivals. As can be seen, interpretation of individual waveforms could vary. What is important is the fact that the combination of the edge effects make up the release portion of the soil stress. Spall initiation, identified by the arrival of the -1 g dwell, occurs after the reflected shear release wave arrives. Initial motion of the reflected shear wave is upward; however, the acceleration decreases slowly and becomes negative. The negative acceleration appears to be limited by the lack of strength of the material to -1 g. If a more competent material was being tested, it is felt that the acceleration could become more negative. Spall initiation has a rapid apparent vertical velocity, implying a nearly horizontally traveling wave.

The fact that the initiation of the spall is, at any particular location, not instantaneous with respect to time, as compared to classical spall (Parret, 1978 (Ref. 7); Eisler and Chilton, 1964 (Ref. 9)), but rather a part of a wave train is helpful in deciding on its cause. In addition, the fact that the spall appears not to travel vertically with a proper wave velocity also helps to rule against classical spall.

Integrated accelerations of longer time durations (Fig. 4), for the same vertical cross section of DH-1 show similar motion. The first motions are

initially down, followed by upward release, a velocity equal to $\int -1 g dt$ and finally a rejoin. During the entire time the relief effects are arriving, the velocity waveform indicates a smooth release. The initiation of the spall is gradual and is observed from the surface to a depth in excess of the radius of the test-bed. Extrapolation of the data indicates that spall reaches to perhaps $1\frac{1}{2}$ times the test-bed radius. Near the surface, the spall phase is followed immediately by a rejoin. At depths greater than 6 m, the rejoin is more complicated. Taking the record at -15 m, (Fig. 4), the free fall is terminated, not by a sharp rejoin but return to a constant downward velocity on the order of -1.2 m/s. A constant velocity of course, indicates zero acceleration. This terminal velocity lasts for approximately 100 ms and is then terminated by a rejoin. The physical explanation of the terminal velocity is unclear and does not always appear in all of the test-beds. The rejoin apparently starts at the surface and works its way down at an apparent velocity varying from 3400 m/s to 287 m/s. Unfortunately the DH-1 had only vertical sensing gages beneath the test-bed. On the other hand, SIMCAL III with limited vertical ranges, does have good coverage in the horizontal direction both within and outside of the test-bed. On the other hand, SIMCAL III, with vertical ranges, does have good coverage in the horizontal direction. For SIMCAL III, information obtained from the limited vertical compares well with the DH-1 (Figs. 4 and 5). Horizontal motion from SIMCAL III is predominantly outward. During the spall phase horizontal accelerations drop to zero as required by the criteria; however, there exists some small horizontal velocity. This indicates the material that is spalled moves both upward and outward. Beyond the test-bed, which ends at a range of 11 m, spall is apparent and is the major vertical motion.

Times of arrivals measured by knowledge of first motion directions were picked and compared to a simple theoretical model (Fig. 6). Because dry alluvium, which at these high pressures is known to be highly nonelastic and nonlinear, a word about the theoretical model is necessary. Upon initial loading, the stress wave will react elastically and travel with a seismic velocity (V_p). As stresses increase, the stress strain curve breaks, giving a substantially lower modulus (Fig. 7). The stress wave will travel at a loading wave velocity (V_L) of approximately 0.4 of V_p up to a point where the

air filled voids are lost (on the order of 100 to 200 MPa). At any point where unloading and subsequent reloading occurs, the stresses will travel at an unloading velocity (V_{up}) that is near the original seismic velocity. For this problem, a trilinear material model will be assumed where the initial uniaxial strain loading will travel at V_p , the peak stress at V_L and the volumetric relief effects at V_{up} made equal to V_p . Comparison with actual in situ data (Fig. 7) indicates that this is not a bad assumption. The shear modulus is assumed to be directly proportional to the constrained modulus through a Poisson's ratio of 0.33. Note that neither the model nor the real physics will allow any relief effects to travel faster than initial loading velocity, although the speeds can cause stress release of the initial compression. The simple model that was used was:

$$\begin{aligned} V_p &= 700 \text{ m/s} \\ V_L &= 280 \text{ m/s} \\ V_{up} &= 700 \text{ m/s} \\ V_s &= 330 \text{ m/s (Poisson ratio} = 0.33) \end{aligned}$$

which appears to fit the data (Fig. 6) well, with the exception of the shear waves. The initial shear wave appears to travel at 330 m/s beneath the explosive cavity in highly disturbed material. The shear velocity increases to 380 m/s outside of the test-bed in less disturbed material.

Spall initiation travels in the horizontal direction at an apparent velocity of 560 m/s. Since this apparent velocity is less than the volumetric reloading P-wave velocity, it must be a shear wave traveling obliquely to the horizontal. An obliquely traveling P release wave would travel at a velocity greater than the true P release wave. For SIMCAL III, at this particular depth, the -1 g dwell is immediately followed by soil rejoin; there is no terminal velocity noted as in DH-1.

Figure 5 shows that under the explosive array the displacement is downward, followed by upward and outward vectors until the spall commences. The outward displacements, however, are only from 5 to 10 percent of the vertical. Outside the test-bed at a range of 7 m from the edge of the explosive array (Fig. 8), initial displacement is outward and down. The motion then becomes

approximately elliptical and retrograde with respect to the direction of propagation until spall initiation, at which point the horizontal velocity drops to nearly zero. The displacement vector suggests that spall is directly preceded by a Rayleigh surface wave, however, these motions were observed in an area that still is undergoing nonelastic strains. In other words, the motions are still probably a direct result of the source, but are clearly in the transition zone between nonelastic source effects and true geologic influences. No data exist to properly define the transition zone for HEST tests.

A vertical profile of displacement time histories was provided by DH-1 (Fig. 9) by doubly integrating accelerations. The number to the right of each curve indicates the depth from which the data are taken. Differences between the data traces at particular times are proportional to the volumetric strain through the spatial derivative. Initial motion of the test-bed is downward, with peak strains occurring near the surface. Upon release, the material remains crushed up, with little strain rebound as expected with alluvium. Spall occurs with the material still under initial compaction, although the material is in tension. From the surface to approximately 5 m in depth, the material regains some of its initial volume, however, below 6 m the entire test-bed remains compacted during the spall and fallback to the position obtained during initial compaction.

In dry alluvium, spall, implying tensional failure, does not imply bulking of the material. The initial stresses are sufficient to cause significant permanent and irrecoverable compaction. This phenomenon is material dependent and is not expected to occur in materials which do not contain large amounts of air filled voids.

To see if spall is common among dry alluvial sites, DISC-1, DISC-2 and DAT-3 were checked (Table 1). In all cases, spall very similar to what has been described existed (Fig. 2). Individual specific material properties varied from site to site (Fig. 7); however, they all exhibited the general alluvial bilinear material behavior. All of the tests were approximately the same size, so that an idea of the dependence of spall with respect to test size could not be attempted.

IV. CALCULATIONS

To obtain better insight into the problem and to be able to identify the causes and effects of the spall, several calculations were performed. The problem deals with material response to shock conditions in a highly non-elastic and nonlinear region of material behavior. In addition, tensile failure and cracking are an important aspect of the problem. As a result, no attempt has been made to model the problem with the usual elastic closed form solution (Murphy 1979 (Ref. 14), and Day et al, 1983 (Ref. 15)). Rather a two-dimensional finite difference, general computer code modeling energy and mass conservation was chosen (Trulio, 1966 (Ref. 16) and Schuster 1982 (Ref. 17)) to investigate the data.

The problem is set up with symmetry about the central axis of the test-bed. For most of the tests, except SIMCAL III and DAT-3, this was the field configuration. To calculate square or rectangular test-beds accurately a two-dimensional code even employing plane strain would be inappropriate because of the four edge boundaries. Recent work (Shinn 1983 (Ref. 18)), however, has indicated that to a first order approximation, an axisymmetric calculation represents square test-beds adequately. In addition, by using a simple geometry individual waves could be studied from a particular boundary without having to contend with traveling waves from additional boundaries.

A Lagrangian formulation was chosen to prevent mixing and loss of material near the areas of large deformations. The grid was to slide on the axis of symmetry, free at the soil-air interface and transmitting at the remaining sides. The grid was made large enough to prevent any spurious grid boundary reflections from causing perturbation in the zone of interest for the duration of the problem. The explosive cavity was simulated by reasonably matching experimental pressure wave forms from SIMCAL III with:

$$p = p_0 e^{-\alpha t} + p_a, X < 7 \text{ m (HEST boundary)}$$

$$p = p_a, X > 7 \text{ m}$$

where

$$p_0 = 10 \text{ MPa}$$

P_a = Atmospheric pressure

α = 500 for the plastic case
 50 for the elastic case

t = Time (in seconds)

The equation of state of the material, modeled with the AFWL engineering model (Shuster 1982 (Ref. 17)), fits the uniaxial strain versus stress data of the material with a series of three straight lines. Plastic flow in shear is allowed when the stress difference exceeds a Drucker-Prager failure criterion given by:

$$\frac{\sigma_1 - \sigma_3}{\sqrt{3}} > C_0 + \beta \bar{P}$$

where

σ_1 = Maximum Principal Stress

σ_3 = Minimum Principal Stress

C_0 = Cohesion

$\beta = 0.7$

$$\bar{P} = \sum_i \sigma_i / 3$$

Plastic flow is modeled as nonassociative, keeping \bar{P} constant when calculating plastic strain. A simple cracking model with appropriate volumetric adjustments is allowed when tension exceeds τ_0 , the tensile limit. Although this model appears to be quite simple it has successfully modeled many high pressure explosive events and is adequate for our purposes.

Three basic calculations were accomplished with the plastic-elastic model shown in Figure 7. Their basic difference was the C_0 used for limiting the plastic flow. In addition, an elastic calculation was done. The elastic-plastic soil model was chosen so that the elastic P wave velocity is equal to the unloading wave velocity of the plastic case. All of the release phenomenon in the plastic calculations should appear to travel at the same velocities as in the elastic case. Comparisons can then be made between the two calculations with respect to wave arrivals, causes and effects.

The calculated velocity vectors at 38 ms into the problem, for the elastic case clearly shows the expected waves (Fig. 10a). The pressure pulse was made short so that it would not obscure the phenomenon. Individual arrivals are labeled with direct waves referring to those generated by the HEST boundary located in the problem; reflected waves refer to those generated by the image boundary or reflected from the center of the asymmetric problem.

The first motions are those observed in the data. The direct P-wave is centered around a P-nodal plane extending directly beneath the boundary of the HEST. First motions of this P-wave are reversed from beneath the HEST to the outside. The action of the shear waves rotating the material upward beneath the explosive cavity is clearly seen. The arrival of the shear wave beneath the test-bed is oblique to the surface as the data suggest.

Figures 10b, c, and d, show velocity vector plots for the three plastic cases at approximately the same times. The pressure pulse was increased in impulse to replicate actual test data better. The arrival of the individual waves are not as clear as in the elastic case. The major difference in the velocity field between the three elastic-plastic calculations is changes in the plastic flow surface through changes in the modeled unconfined C_0 . The unconfined cohesion essentially dictates the allowed limit of stress difference allowed. Although simply modeled, it appears to be an adequate representation of the observed physics.

The calculations indicate that, for material having less cohesion, the shear wave becomes progressively less strong and is absent from the calculation with no cohesion. For the case with zero cohesion, the material under the explosive fails to rebound substantially, and fails to obtain any upward velocity. Instead, plastic flow dominates and the test-bed material flows downward and outward from the test-bed. Observations showing this behavior have been noted in large HEST tests fired over saturated clayey soils with little cohesion. As the modeled cohesion is increased, the material is affected more by the shear wave and is seen to obtain upward velocities which terminate in tensional failure and spall. Spall then appears and can be associated with shear wave action. The presence or absence of spall is directly related to the modeled cohesion of the material.

With the model employed, material cracking is noted (Fig. 11) both beneath and outside the explosive cavity. Initial compression causes shear failure (in the material with high cohesion) or plastic flow (material with zero cohesion), allowing material to move both downward and outward. The arrival of the direct and reflected P- and S-waves causes the test-bed to be thrown upward ending in tensional failure or spall as shown by the horizontal crack indicators. The shear wave appears to be a significant factor in causing spall, implying that unconfined cohesion of the soil is required for spall to be initiated by a shear wave. The region of spall in the calculations extends to approximately $1\frac{1}{2}$ times the radius of the explosive cavity agreeing with extrapolation of the data. As with the data, failure is also observed outside of the test-bed. The failure occurs rapidly, as seen in the data, requiring only a few cycles of the calculations.

Vertical velocity time histories for four cases of different C_0 clearly show the effects of the shear wave interaction (Fig. 12) on the final velocity time history. The time histories shown are for the centerline of the test-bed so that the direct and reflected waves arrive simultaneously. The time histories again show what has been described before. Spall initiation, identified by a constant slope in the velocity field equal to -1 gt, does not occur at initial shear arrival but is delayed until the positive vertical velocity is sufficient to cause failure. The plastic case having no cohesion does not appear to permit shear wave propagation, resulting in small velocity reversals.

The P-wave nodal plane generated by the finite boundary is clearly seen in the calculation. Near the surface, almost no P-release wave motion is observed. As one goes deeper, the amplitude increases. However, if stress time histories are plotted, the effect of the P-release wave is clearly seen. The normal stresses are substantially reduced to zero.

V. DISCUSSION AND CONCLUSION

The importance of this work is to uniquely identify a physical process that produces a spall waveform, which is not dependent upon the classical reflection of a compression wave. As early as 1966, Chilton, et al, (Ref. 12) suggested alternatives to the classical theory. A great deal of interest was shown when spall identified with surface explosions could not be related to the classical explanation (Merkle, 1980 (Ref. 6); Stump and Reinke, 1983 (Ref. 5); Day, et al, 1983 (Ref. 15) and Auld and Murphy, 1979 (Ref. 19)). As a result, four additional mechanisms have been proposed by Stump and Reinke (1983) (Ref. 5), in addition to the classical mechanism. This particular data set is of interest because the final motion resulting from a dynamic uniaxial compression test is tensional failure and spall. Clearly, the tensional failure cannot be caused by a compressional wave traveling upward to the surface and reflecting. This required an alternate theory which allows large velocity reversals through shear wave interaction upon release of the soil stress.

With a HEST-type loading it is tempting to relate the observed spall with a surface point source. As one gets away from the test-bed, the HEST approximates a point source. Aki and Richards (1980, p 218) (Ref. 13) illustrate the generation of shear waves from a surface point source by using a torus with downward and outward rotating motion. In a sense, the circular HEST may be considered as just such a geometric array. The calculations indicate that major shearing exists during this initial compressional phase outside the test-bed as indicated by theory; however, it is the release wave from the edges of the test-bed that cause rotation and upward motion that results in spall. For a point source explosive, the edge effects are not as clearly defined as for the HEST. However, at any particular instant in time, the overhead airblast from a surface burst does have finite boundaries associated with the airblast. The finite boundaries, although moving, would cause an initiation of a shear wave. Thus spall associated with airblast can be postulated to exist. In addition to the airblast, spall from bermed explosives without airblast are also observed (Fig. 2). The spall mechanism observed with the bermed charges is in addition to the spall due to the airblast and is probably due to the same shearing mechanism.

Comparison of data and calculations indicates that the spatial extent of the spall, and thus its initial duration, or wave length, are directly proportional to the size of the HEST. Both the data and calculations indicate that the extent of spall in a vertical direction is approximately $1\frac{1}{2}$ times the radius of the HEST. Extending this to a surface burst would imply that the vertical extent of spall is related somehow to the peak overpressure areal history. Since the overpressure scales as the cube root of the energy of the point source, the extent of the spall on a surface burst could also scale as the cube root of the yield. However, the tensional stress required to cause spall would appear to increase due to increased lithostatic pressures.

Another important result from this data is the relationship between strength or C_0 of the soil and the resulting upward vertical velocity attained just prior to the initiation of spall. Figure 11 qualitatively describes the limits of peak upward velocities obtainable for various C_0 's. No upward velocity for soil modeled with zero cohesion to large upward motions for elastic material were calculated. A ratio of peak upward velocity calculated compared to the peak downward velocity was found to be related to the cohesion of the soil model (Fig. 13). In addition, the qualitative appearance of the spall initiation is also related to the modeled cohesion. The calculations indicate that the cohesion of 0.5 MPa produced a sharper spall initiation than one of 0.3 MPa. Ratios of the velocities can be made using data which indicate that, for soils tested, a cohesion of 0.3 MPa to 0.5 MPa is required to model the spall signature.

For dry alluvial soil, these cohesions appear a bit large. On the other hand, a true in situ estimate of cohesion is one property that remains almost unmeasurable with available techniques (A. E. Jackson, personal communication). In addition, the materials for which these estimates are made have been initially compacted. The displacement time histories (Fig. 9) also show that tensional failure occurs while the material is still under uniaxial strain. This also may affect the final cohesion of the soil, before spall. Although the relationship between cohesion and spall signature is now only an observation, it may prove to be an important measure of soil cohesion.

Spall and tensional failure is observed in uniaxial dynamic compression material properties tests, apparently a result of shear waves generated from

the finite boundaries of the experimental test-bed. Calculations, both elastic and elastic-plastic, using simple soil models have helped to confirm the phenomenon. The spall signature is much different from that observed from classical reflection of compressive stress waves impinging upon a free surface. The phenomenon may be applicable to surface point sources. Finally, calculations indicate that the spall signature and the ratio of peak upward velocity versus peak downward velocity may be directly related to the cohesion of the dry alluvium.

- ① DIRECT P
- ② DIRECT S
- ③ REFLECTED P
- ④ P-S
- ⑤ REFLECTED S

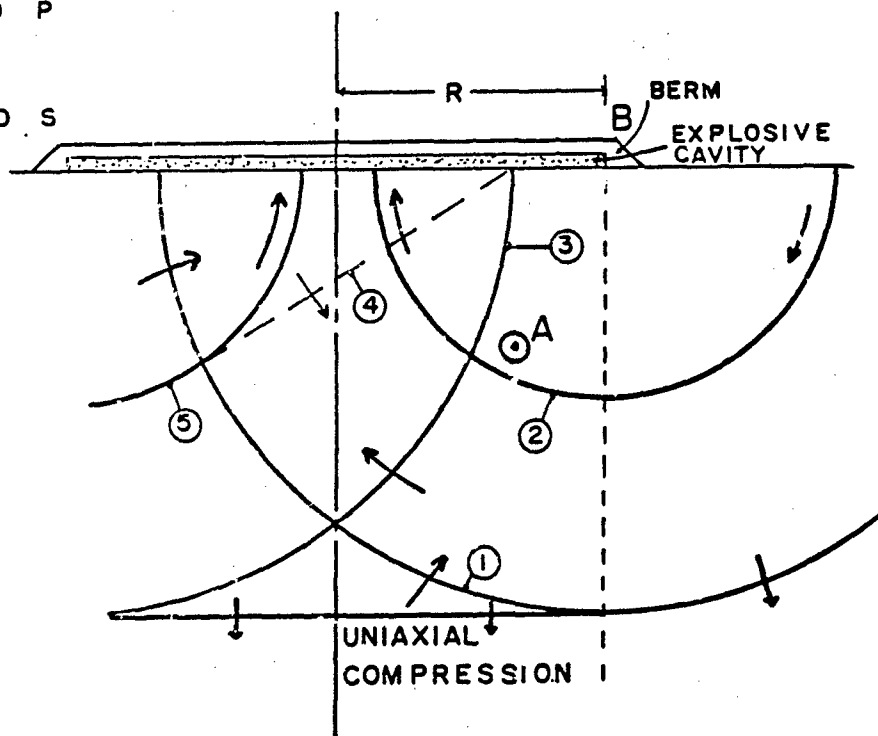
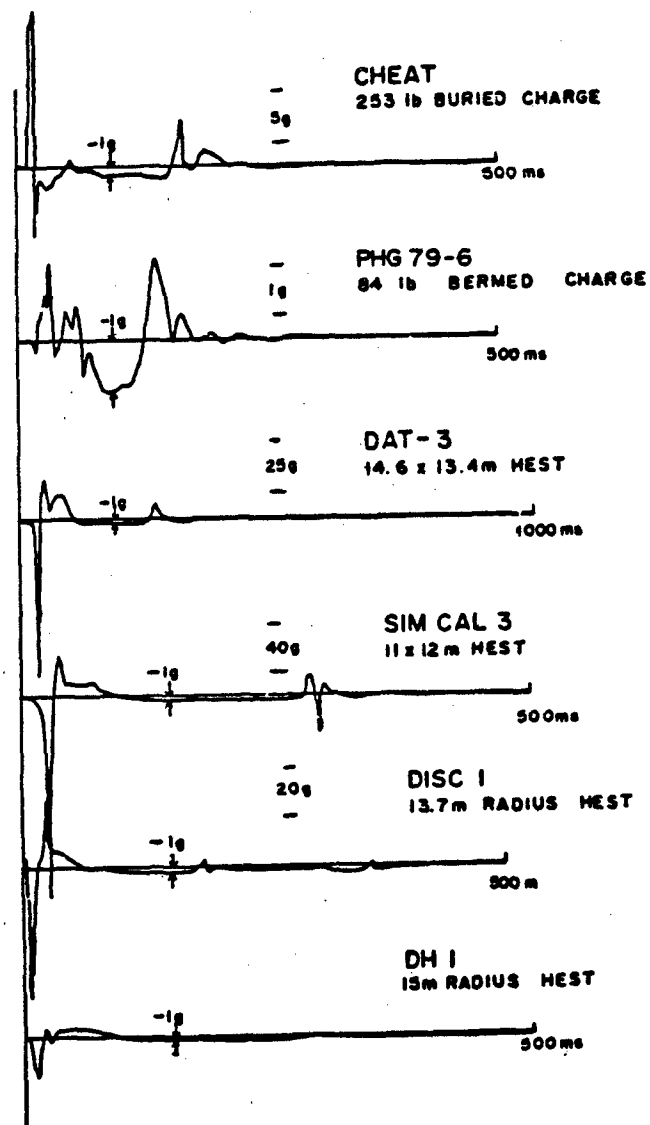


Figure 1. Test configuration showing typical test-bed and wave fronts. (The arrows indicate the direction of first motion.)

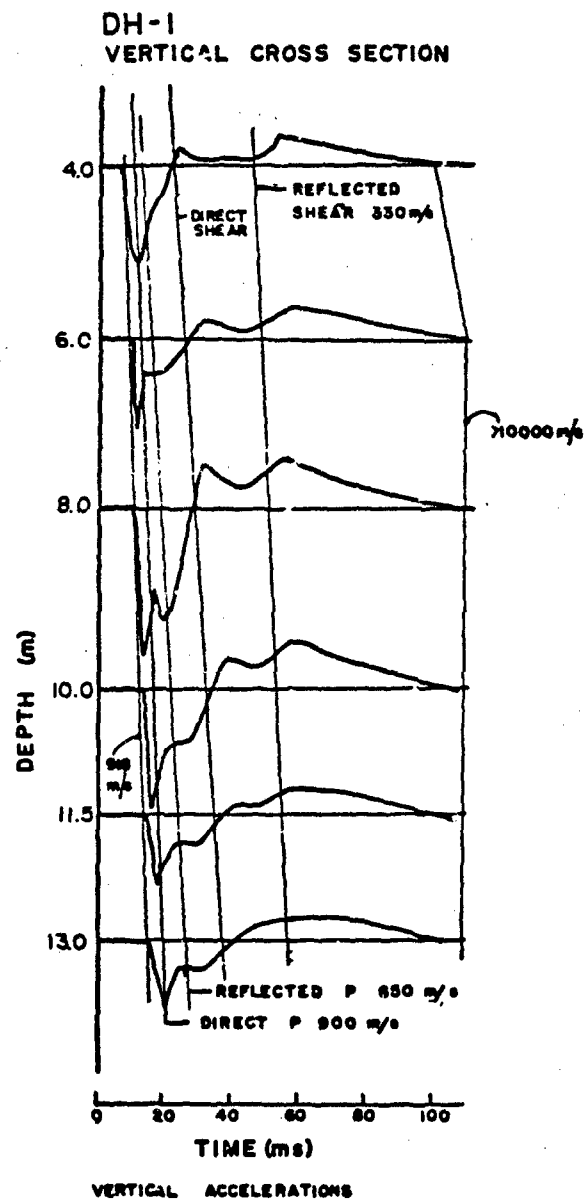


VERTICAL ACCELERATION

Figure 2. Acceleration records from six HE tests showing two different types of spall signature.

TABLE 1. SIZE, LOCATION AND PRESSURE PULSES FOR 5 HEST TESTS (Refs. 2 & 3)

Test	Geometry	Dimensions (m)	Soil Type	Overpressure (MPa); t = sec
SINICAL III	Rectangular	X=24; Y=22	Yuma Dry Alluvium	$9.5 \left(0.54e^{-43.4t} + 0.46e^{-240t} \right)$
DH-1	Circular	R = 13.7	Navada Test Site (NTS)	$4.29 \left(0.71e^{-34t} + 0.29e^{-858t} \right)$
DISC-1	Circular	R = 13.7	Ralston Valley NV (RV)	$10.2 \left(0.47e^{-26.7t} + 0.52e^{-173t} \right)$
DISC-2	Circular	R = 13.7	Ralston Valley NV (RV)	$10.2 \left(0.47e^{-26.7t} + 0.52e^{-173t} \right)$
DAT-3	Rectangular	X = 14.6; Y = 13.4	Rio Grande Valley III (RGV)	$14.0 \left(0.32e^{-90t} + 0.68e^{-2000t} \right)$



NOTE: The four release waves and spall initiation are shown. Records are truncated at spall initiation. See Figure 4 for longer time durations.

Figure 3. Vertical accelerations from DH-1 for a cross section 3 m from the centerline of the HEST.

TABLE 2. PARAMETERS USED IN THE CALCULATIONS

Calculation	Type	V_p (m/s)	V_L (m/s)	V_{up} (ms)	C_o (MPa)	Poisson's Ratio
1	Elastic	800	800	800	N/A	1/3
2	Plastic	550	333	800	0.0	1/3
3	Plastic	550	333	800	0.3	1/3
4	Plastic	550	333	800	0.5	1/3

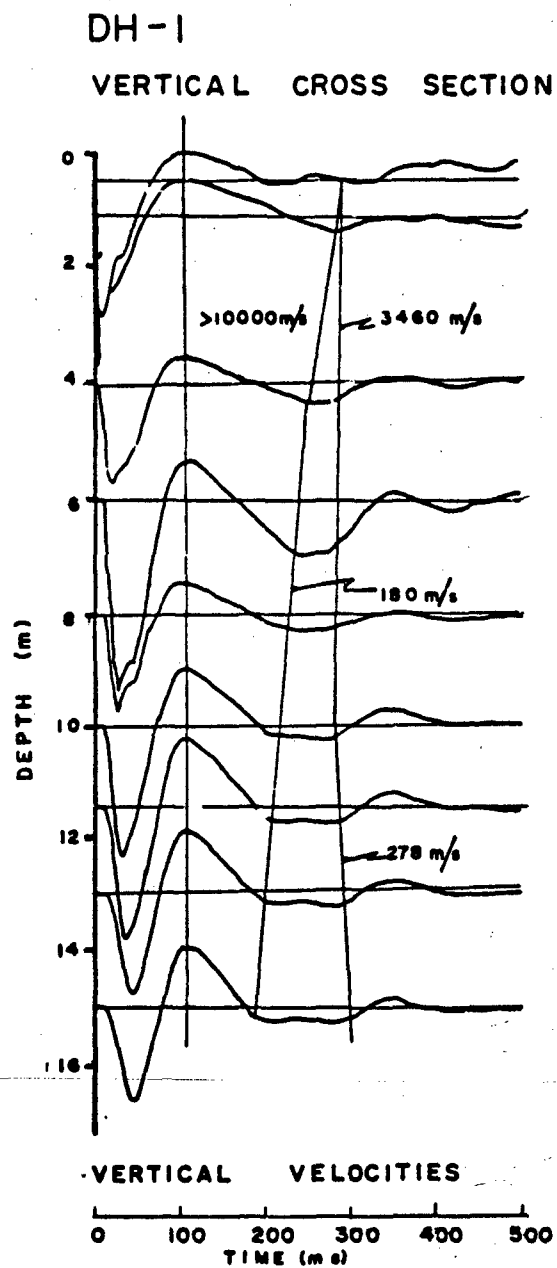


Figure 4. Velocity time histories from DH-1. (The location of the cross section is 3 m from the centerline.)

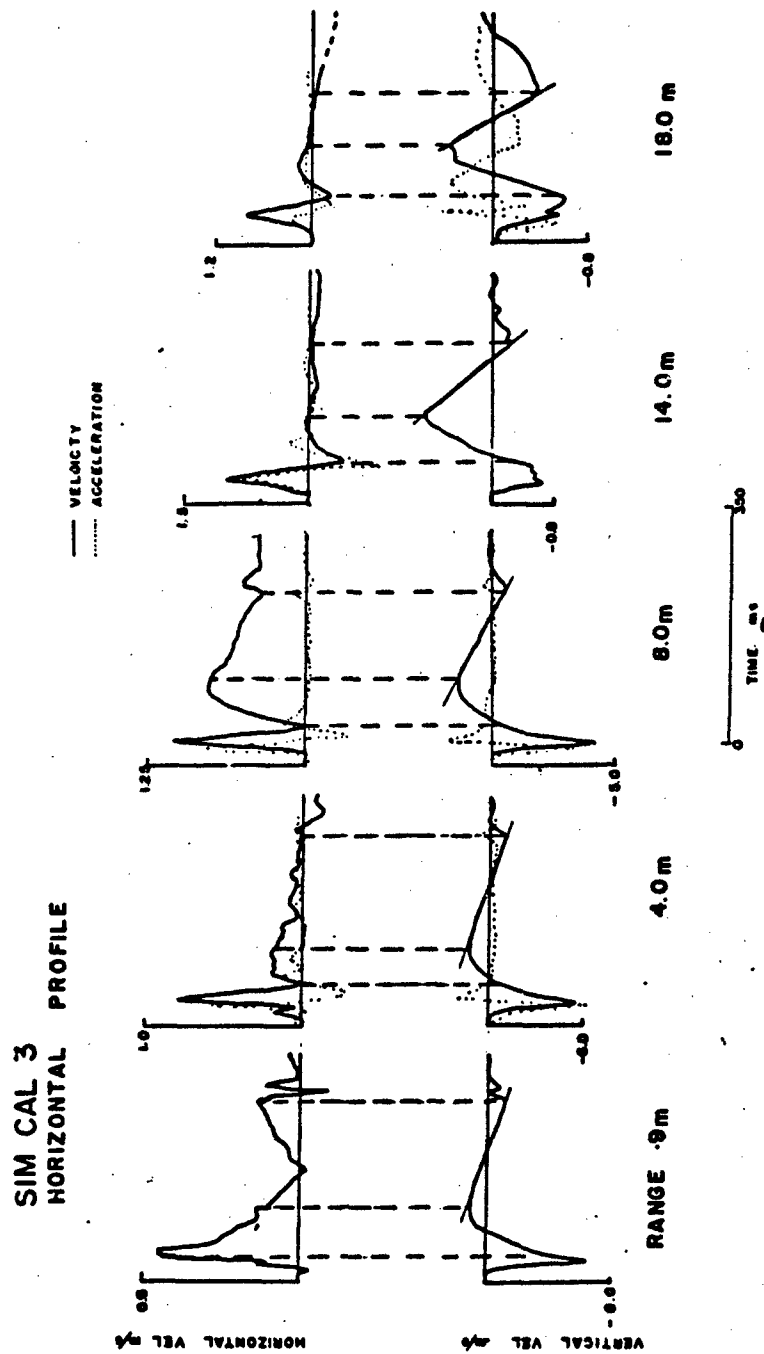


Figure 5. Horizontal and vertical acceleration waveforms at a constant depth of 5.4 m for SIMCAL III. (The test-bed edge is located 11 m from the centerline located at 0.0 m.)

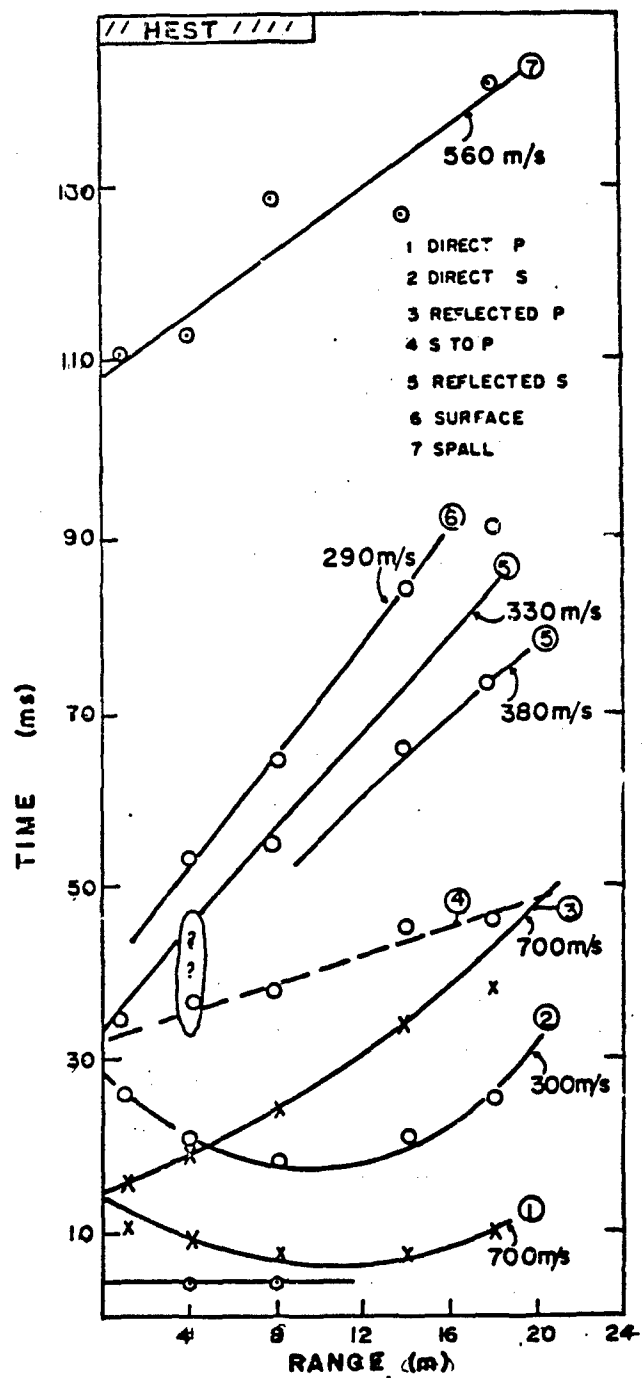


Figure 6. Times of arrivals for various waves from SIMCAL III (data points). (The solid lines indicate model solution.)

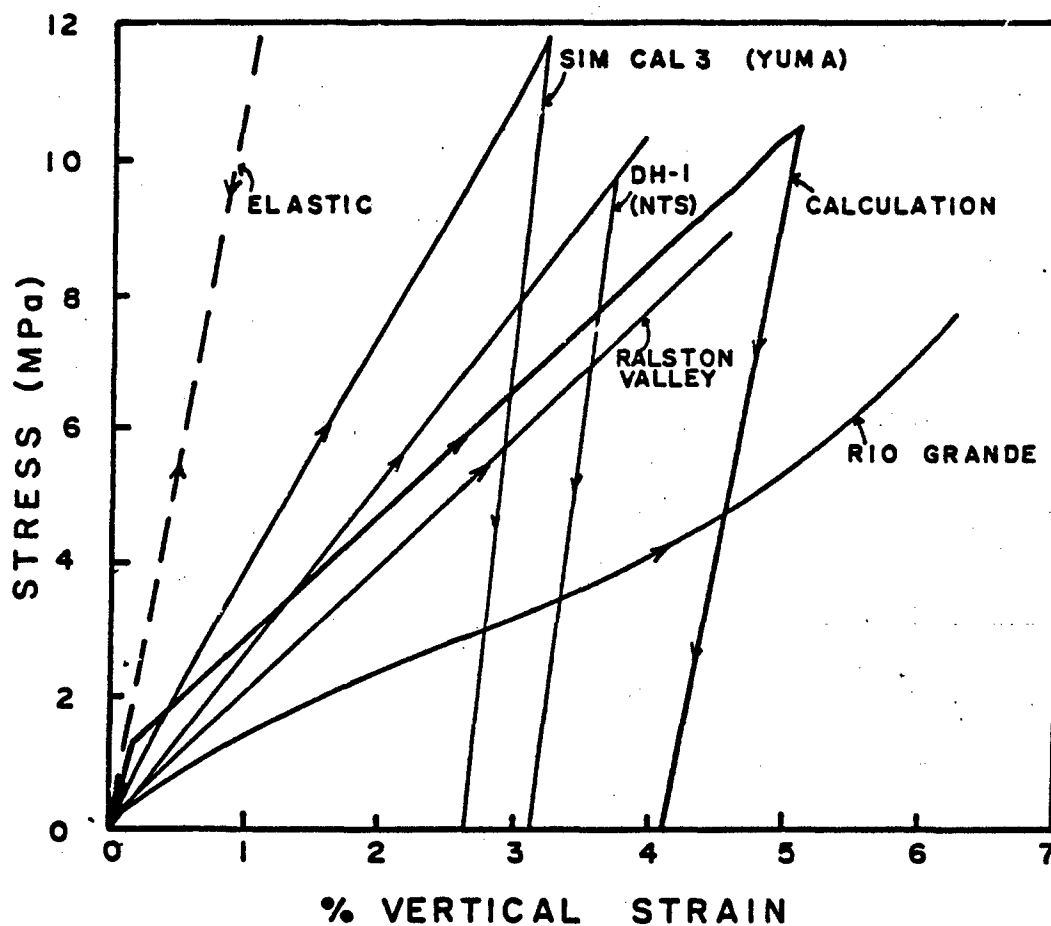


Figure 7. Uniaxial strain in situ material models estimated for the various sites. [Also shown are the two (elastic and elastic-plastic) models used in the calculation.] (After Ref. 2.)

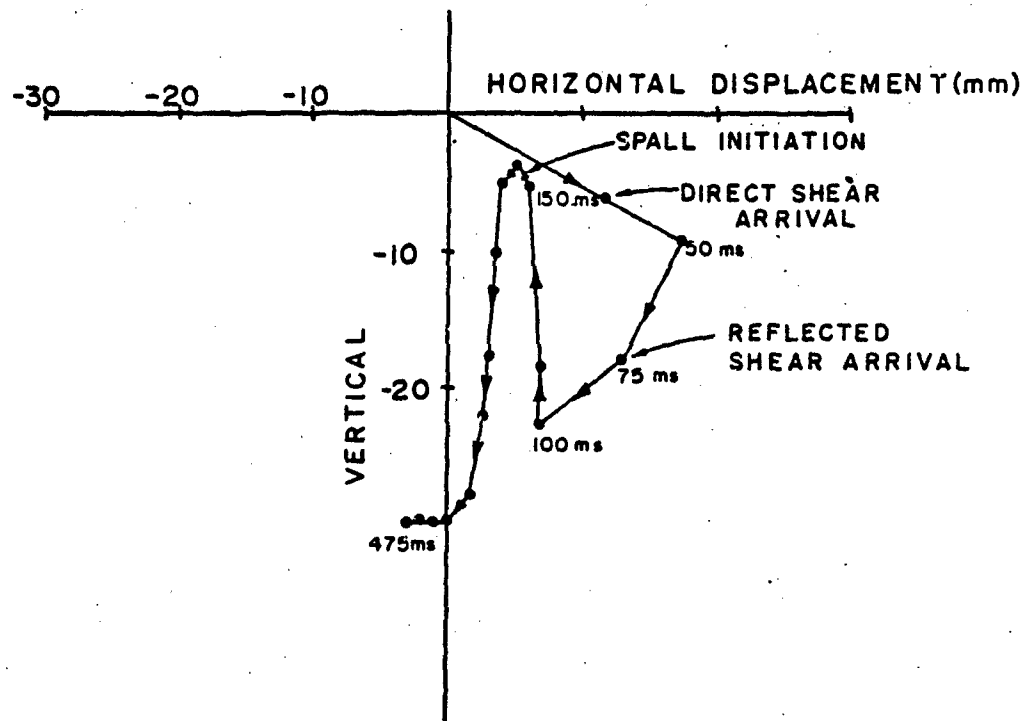


Figure 8. Displacement map of a superposition of both horizontal and vertical displacements. (This is for a station 7 m from the edge of the test-bed at a depth of 5.4 m for SIMCAL III.)

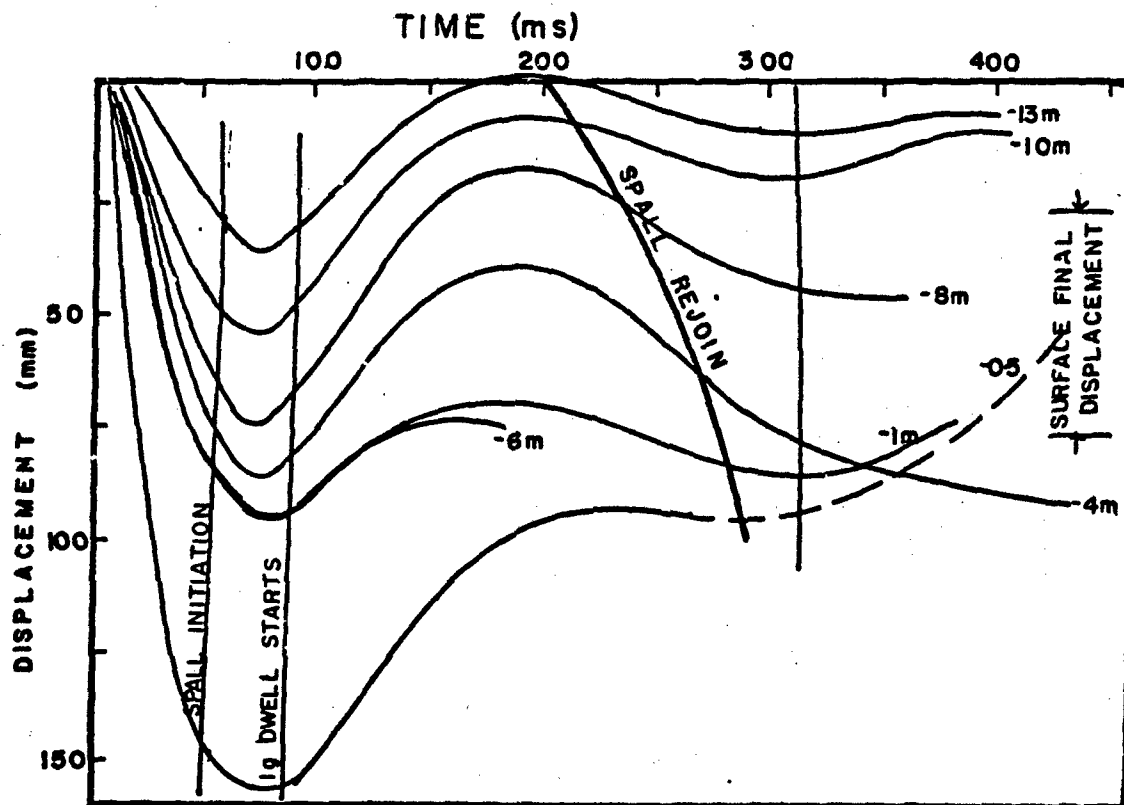
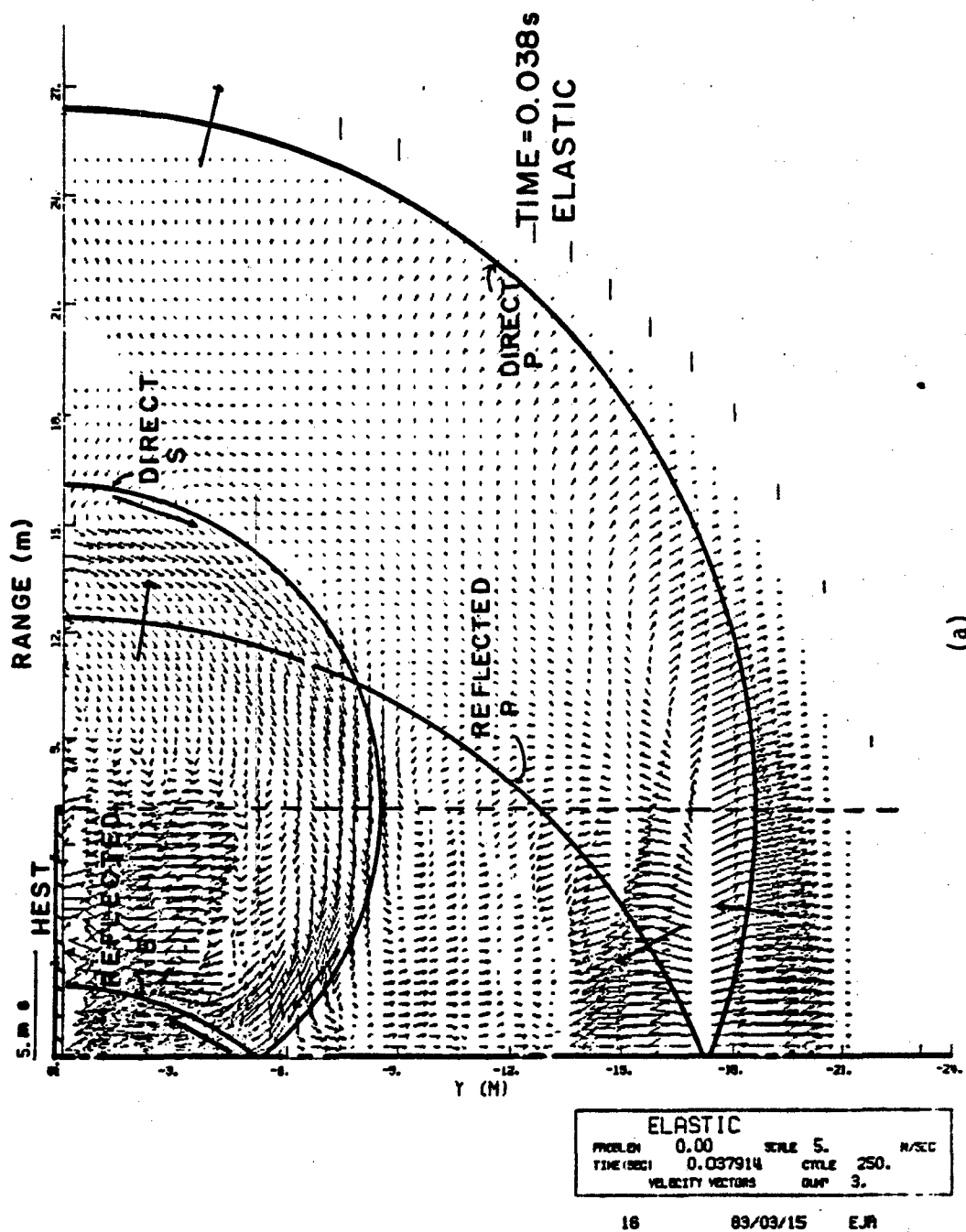


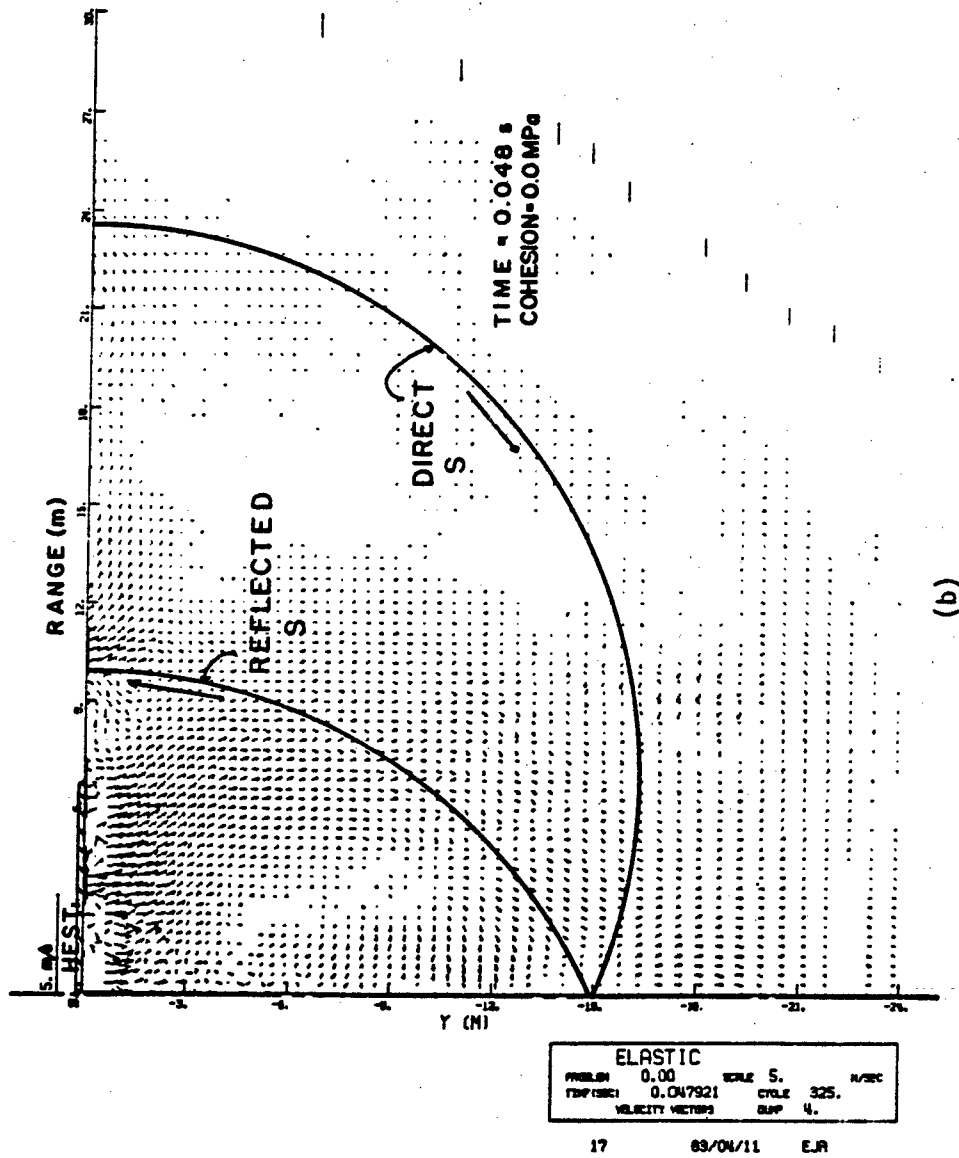
Figure 9. Displacement time histories for DH-1. (Records are from doubly integrated accelerations seen in Figure 4.)



(a)

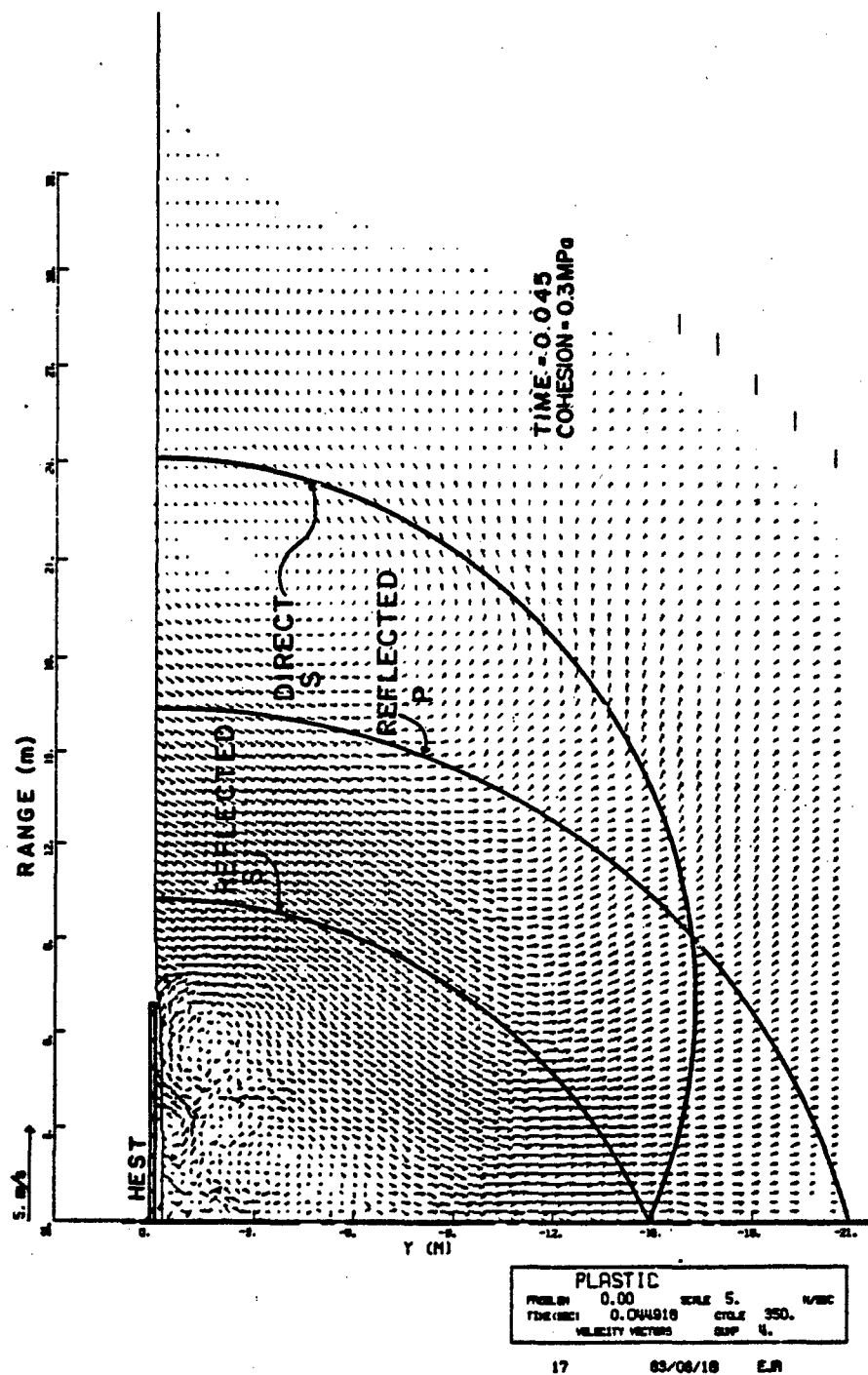
NOTE: Plots are taken at the times when the reflected shear waves appear directly under the test-bed. The modeled cohesion varies from 0.0 MPa to elastic.

Figure 10. Velocity vector plots from the calculations.



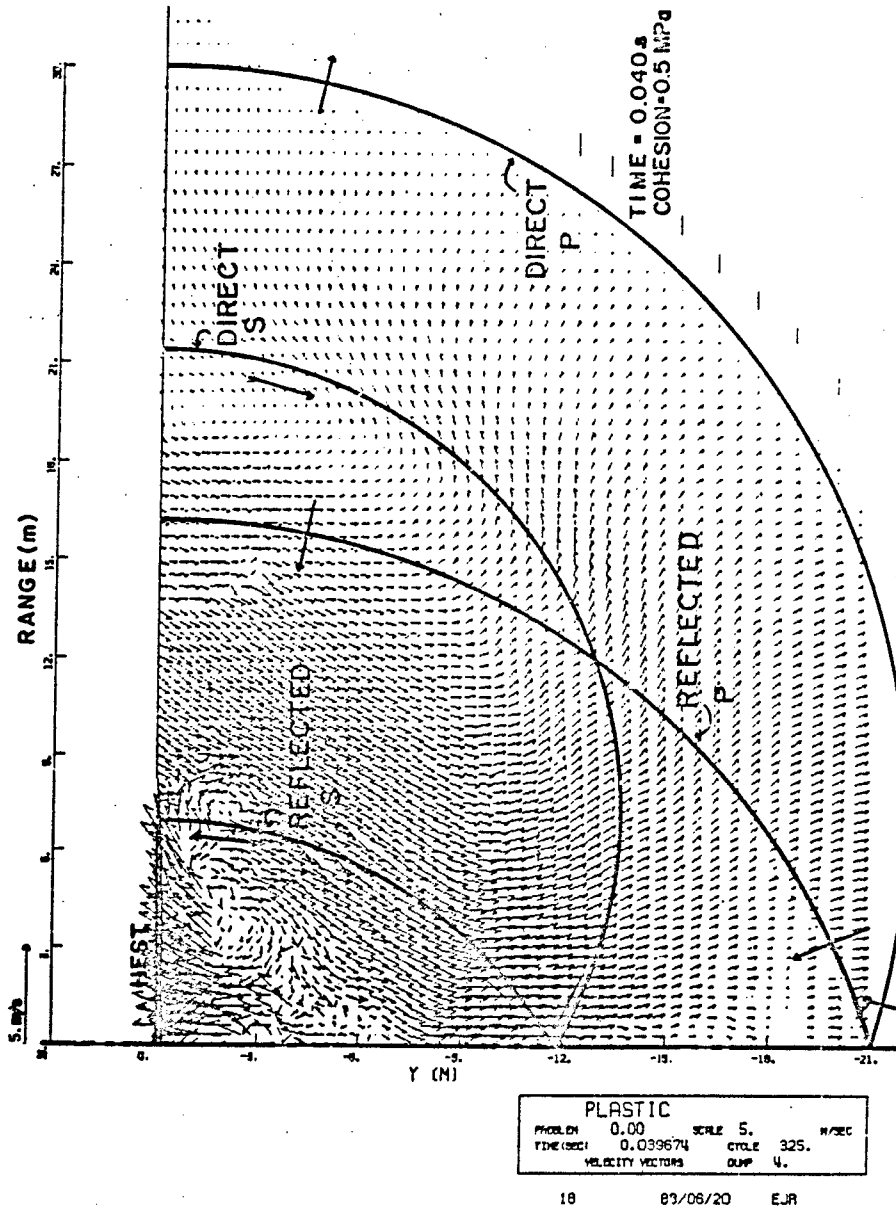
(b)

Figure 10. Continued.



(c)

Figure 10. Continued.



(d)
Figure 10. Concluded.

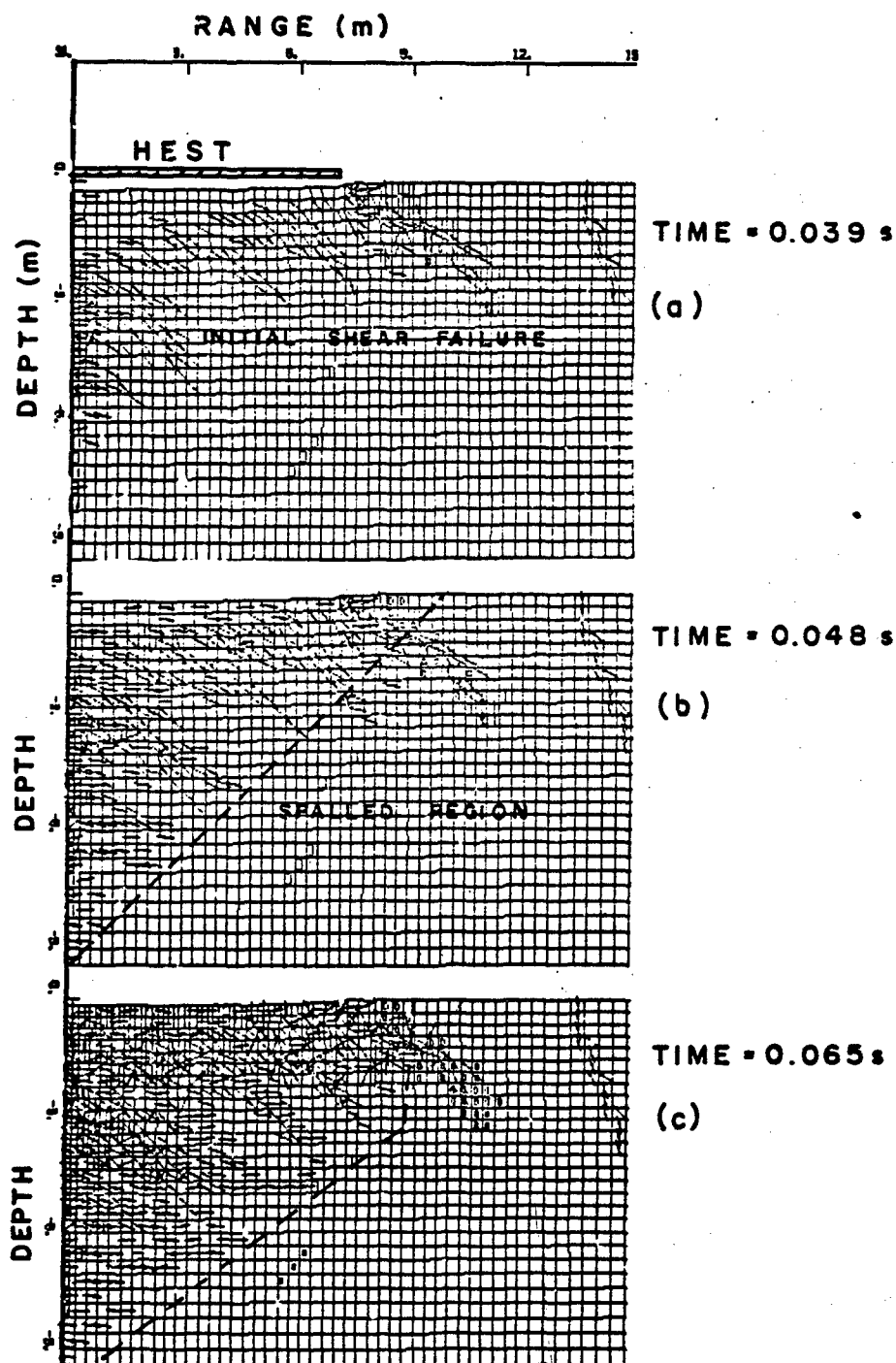


Figure 11. Plot of the grid and fracture pattern at three times for the case where $C_0 = 0.5$ MPa. [The crack symbols (dashes within the grid) are orientated normal to the least principal stresses.]

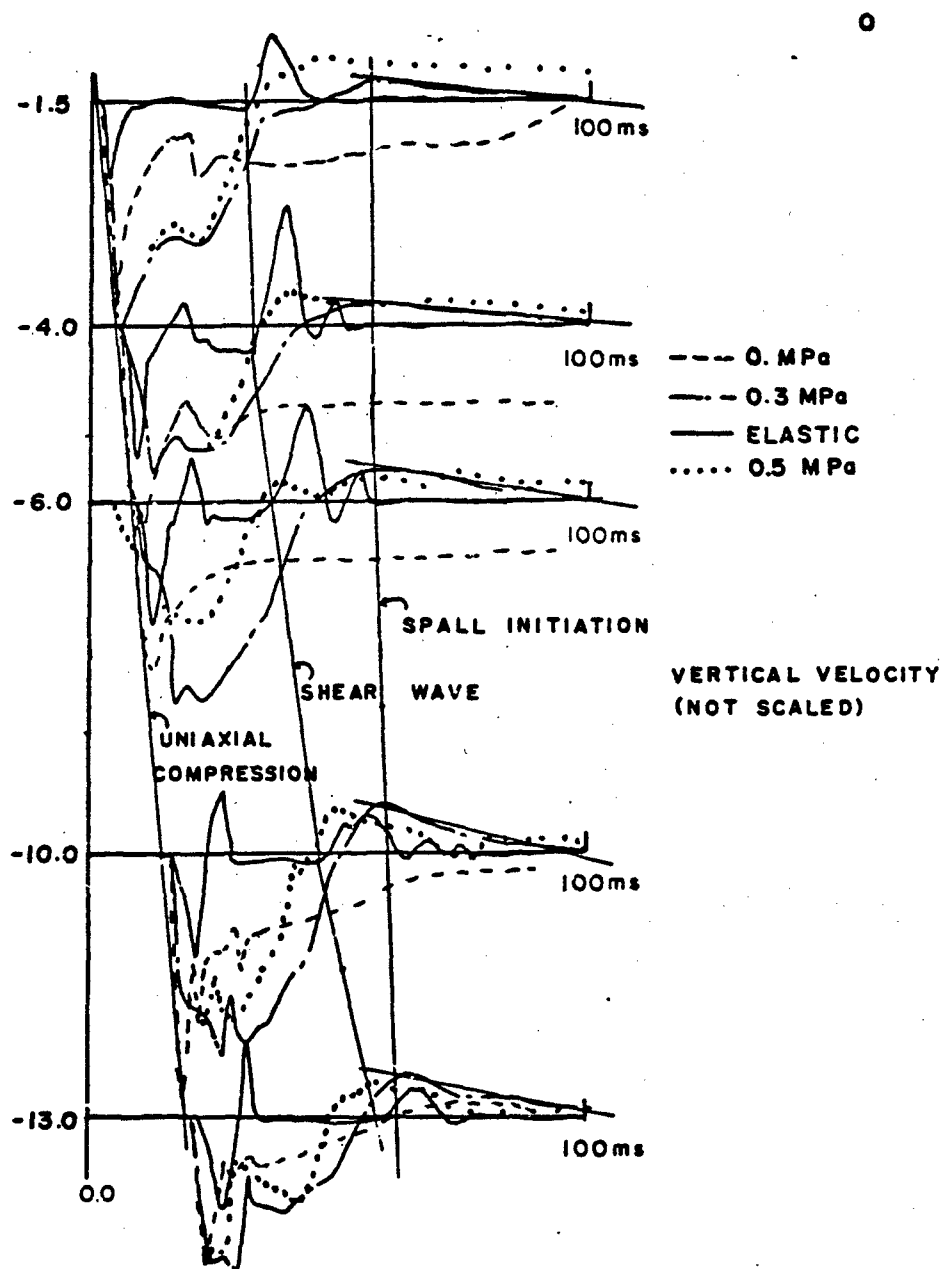


Figure 12. Velocity wave forms at the symmetry axis for four calculations.

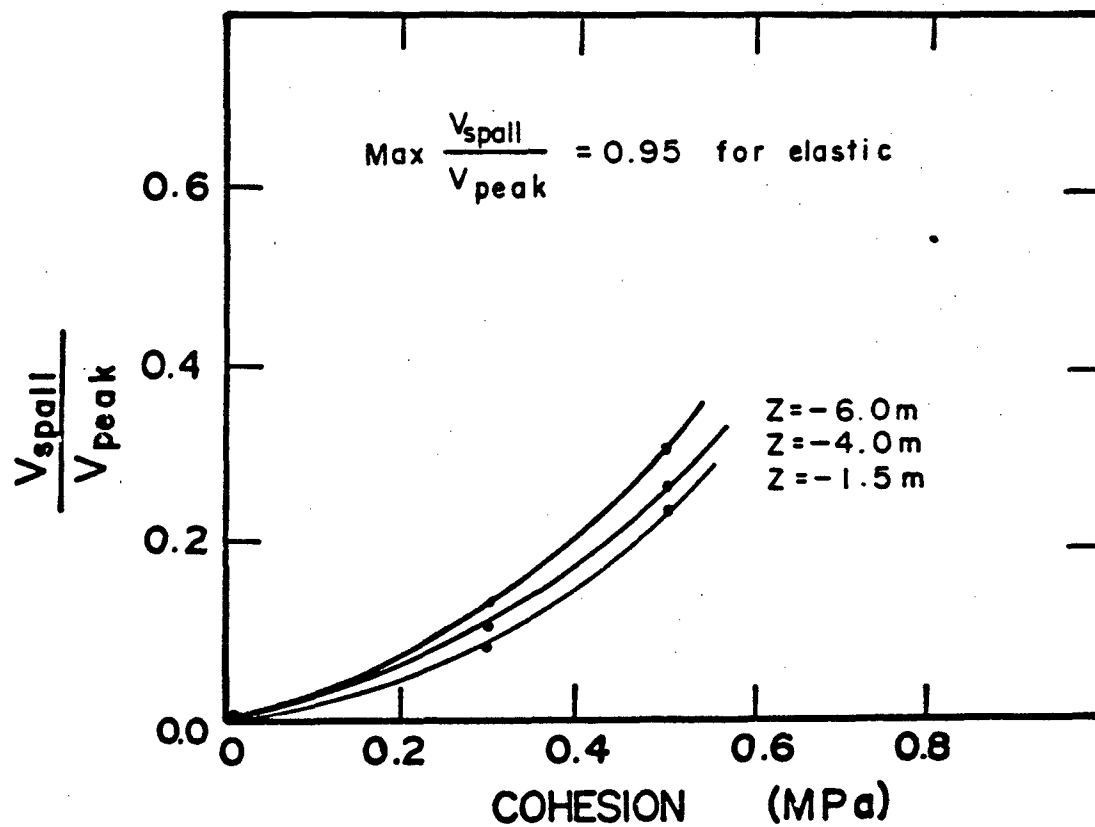


Figure 13. Comparison of peak particle velocity obtained at spall normalized by the peak pressure compared to the modeled cohesion.

REFERENCES

1. Bratton, J. L. and Higgins, C. J., "Measuring Dynamic In Situ Geotechnical Properties in Earthquake Engineering and Soil Dynamics," ASCE Geotechnical Engineering Division, AFCE, New York, New York, 1979.
2. Swartz, L., Noble, M., Edwards, J., Rinehart, E. and Schneider, J., DISC HEST 1 (DH-1), AFWL-TR-81-20, Air Force Weapons Laboratory, Kirtland AFB, New Mexico, 1981.
3. Jackson, A. E., Jr. and Zelasko, J. S., Ralston Valley Soil Compressibility Study: Quick-Look Report for DISC TEST II, U.S. Army Engineer Waterways Experiment Station, Structures Laboratory, Vicksburg, Mississippi, 1982.
4. Rinehart, E. J. and Lucey, R., Ralston Valley Dynamic In Situ Compressibility (DISC 1) Test Pretest Prediction; A 2-D HEST Relief Wave Calculation, AFWL-NTE-TR-81-003, Air Force Weapons Laboratory, Kirtland AFB, New Mexico, 1981.
5. Stump, B. W. and Reinke, R. E., Spall Observations and Mechanisms in Alluvium, submitted to J. of Geophysical Research, 1983.
6. Merkle, D. H., Basic Mechanisms of Spall From Near-Surface Explosions, Final Report for Contract F49620-80-C-0059, Air Force Office of Scientific Research, Bolling AFB, DC, 1980.
7. Parret, W. R., Surface Motion Near Underground Nuclear Explosions in Desert Alluvium Operation Hougat 1, Area 3, Nevada Test Site, SAND7-1439, Sandia National Laboratories, Kirtland AFB, New Mexico, 1978.
8. Rinehart, J. S., "Spalling and Large Blasts," Proceedings of the 2nd Plan Share Symposium, Part 1, pp. 135-155, UCRL-5675, San Francisco, California, May 1959.
9. Eisler, J. and Chilton, F., "Spalling of the Earth's Surface Caused by Underground Nuclear Explosions," J. Geophys. Res., 69, 5285, 1964.
10. Vieceilli, J. A., "Spallation and Generation of Surface Waves by an Underground Explosion," J. Geophys. Res., 78, 2475-2487, 1973.
11. Rinehart, J. S., "Stress Transients in Solids Hyperdynamics," Santa Fe, New Mexico, 1975.
12. Chilton, F., Eisler, J. D. and Heuback, H. G., "Dynamics of Spalling of the Earth's Surface Caused by Underground Explosions," J. Geophys. Res., Vol. 71, No. 24, pp. 5911-5919, 1966.
13. Aki, K. and Richards, P. G., Quantitative Seismology Theory and Methods, W. H. Freeman and Company, San Francisco, California, 1980.

14. Murphy, J. R., "Near-Field Rayleigh Wave from Surface Explosions," Bul. Seismo. Soc. of Am., Vol. 71, No. 1, pp. 223-248, 1981.
15. Day, S. M., Rimer, N. and Cherry, J. T., "Surface Waves from Underground Explosions with Spall: Analysis of Elastic and Nonlinear Source Models," Bul. Seismo. Soc. of Am., Vol. 73, No. 1, pp. 247-264, 1983.
16. Trulio, J. G., Theory and Structure of the AFTON Codes, AFWL-TR-66-19, Air Force Weapons Laboratory, Kirtland AFB, New Mexico, 1966.
17. Schuster, S. H., CRALE User's Manual, AFWL-TR-82-45, Air Force Weapons Laboratory, Kirtland AFB, New Mexico, 1982.
18. Shinn, J. D., II, Relief Effects Beneath Nuclear Airblasts Simulators Conducted Over Dry Alluvial Soils, AFWL-TR-83-31, Air Force Weapons Laboratory, Kirtland AFB, New Mexico, August 1983.
19. Auld, H. E. and Murphy, F. R., "Surface Wave Calculations," Proceedings, DNA Strategic Structures Division Biennial Review Conference, Menlo Park, California, March 1979.

BIBLIOGRAPHY

Analysis of SIMCAL 1, 2, and 3, AFWL-TR-80-42, Air Force Weapons Laboratory, Kirtland AFB, New Mexico, 1980.

Bedsum, D. A., "Geotechnical Investigations of the CHEBS and GAS Test Sites: Madeira Canyon, Kirtland AFB, NM; Letter Report, New Mexico Engineering Research Institute, Albuquerque, New Mexico, 1983.

Karably, L. S., Geotechnical Investigation in Southwestern Arizona, AFWL-TR-78-146, Air Force Weapons Laboratory, Kirtland AFB, New Mexico, 1979.

Phillips, B. R. and Jackson, A. E., Jr., Ralston Valley Soil Compressibility Study: Laboratory Test Results, Informal Report, Waterways Experimental Station, Structures Laboratory, Vicksburg, Mississippi, 1982.

Rinehart, J. S., Stress Transients in Soils, Hyperdynamics, Santa Fe, New Mexico, 1979.

Smith, J. L., Betz, J. F. and Hazen, C., DAT-3 Analysis, AFWL-TR-to be published, Air Force Weapons Laboratory, Kirtland AFB New Mexico.

Triandafilidis, G. E., Calhoun, D. E. and Abbott, P. A., Simulation of Airblast-Induced Ground Motion at McCormick Ranch Test Site, Vol. 1, AFWL-TR-68-27, Air Force Weapons Laboratory, Kirtland AFB, New Mexico, 1968.